Vibrationally Promoted Dissociation of Water on Ni(111)

P. Morten Hundt *et al.*

Science **344**, 504 (2014);
DOI: 10.1126/science.1251277

rapidly and cleanly neutralized. The reaction mixture obtained after the incubation for 48 hours at 25°C showed in DLS a marked increase in apparent hydrodynamic diameter from 11 to 82 nm (Fig. 4J). Therefore, we carried out tapping-mode AFM of an aliquot of the reaction mixture on mica and found that long cylindrical objects are reconstructed (Fig. 4F). These observations indicate that reduced nanorings **FcNR$_1$** are equilibrated with their uniaxially "merged" nanotubular assembly of **FcNT$_1$** (Fig. 1E). The uniaxial merging event of **FcNR$_1$** appears rather sluggish, certainly due to its large entropic loss. When the reaction mixture, incubated for 0.5 hours after the complete reduction of the ferrocene units of **Fc$^+$NR$_1$**, was air-dried on mica and analyzed with tapping-mode AFM, only toroidal objects were visualized (Fig. 4E). Analogous to the case of **FcNT$_1$**, we attempted oxidative cutting of larger-diameter **FcNT$_2$** by using $Cl_2Fc^+BF_4^-$. However, a mixture of ill-defined structures resulted. We consider that **FcNT$_2$** cannot satisfy a requisite for the selective attenuation of noncovalent forces, most likely because of an insufficient structural robustness originating from its large and thin-wall dimensions.

Considering a possible entropic penalty for the formation of giant nanorings through the direct self-assembly of small molecules, we suppose that the Ag(I)–mediated nanotubular assembly of **FcL** (Fig. 1C) probably occurs stochastically, without preceding formation of the corresponding nanorings (**FcNR**). In the crystalline state, tetraarylferrocene derivatives are known to adopt an eclipsed geometry (*29*, *30*). By means of ^{1}H nuclear magnetic resonance (NMR) spectroscopy in CD_3CN, we confirmed that the geometry of **FcL$_1$** in solution is more biased to the eclipsed form at lower temperatures. However, even at –40°C its ^{1}H NMR spectral feature was still dynamic (fig. S5). Meanwhile, when **FcL** is bound to Ag(I) ions a metallophilic interaction may occur, so that its tendency to form the eclipsed geometry is enhanced. The resultant Ag(I)–bound bent-shaped ligands are connected together to form a doubly bridged metal-organic oligomer (Fig. 1B, bottom center). Such oligomers may start to stack up bilaterally via amplified π-stacking and metallophilic interactions. Consequently, curvy sheet-like intermediates would form and grow up stochastically to furnish nanotubular **FcNT$_1$** at the final stage. In regard to the stochastic assembling mechanism thus proposed, neither nanotubes nor nanorings were detected with AFM when oxidized **FcL$_1$** (**Fc$^+$L$_1$**) with an attenuated stacking ability was likewise treated with $AgBF_4$ (fig. S19). As highlighted in the present work, 200-membered metal-organic decagonal nanorings (**Fc$^+$NR$_1$**), obtained by oxidative cutting of the nanotube, are unlikely to form directly with conventional self-assembling protocols. Together with the results of electrostatic pasting (Fig. 1G) and reductive merging (Fig. 1E) of **Fc$^+$NR$_1$**, we believe that the idea of stepwise noncovalent synthesis—involving cutting, pasting, and merging operations—may open additional routes for nanoscale synthesis.

References and Notes

1. J.-M. Lehn, *Supramolecular Chemistry* (Wiley-VCH, Weinheim, ed. 1, 1995).
2. L. J. Prins, D. N. Reinhoudt, P. Timmerman, *Angew. Chem. Int. Ed.* **40**, 2382–2426 (2001).
3. R. Chakrabarty, P. S. Mukherjee, P. J. Stang, *Chem. Rev.* **111**, 6810–6918 (2011).
4. H. Furukawa, K. E. Cordova, M. O'Keeffe, O. M. Yaghi, *Science* **341**, 1230444 (2013).
5. Q.-F. Sun *et al.*, *Science* **328**, 1144–1147 (2010).
6. T. Aida, E. W. Meijer, S. I. Stupp, *Science* **335**, 813–817 (2012).
7. A. Müller, S. Q. N. Shah, H. Bögge, M. Schmidtmann, *Nature* **397**, 48–50 (1999).
8. T. Liu *et al.*, *Science* **331**, 1590–1592 (2011).
9. X. Wang *et al.*, *Science* **317**, 644–647 (2007).
10. T. Gädt, N. S. Ieong, G. Cambridge, M. A. Winnik, I. Manners, *Nat. Mater.* **8**, 144–150 (2009).
11. A. H. Gröschel *et al.*, *Nature* **503**, 247–251 (2013).
12. A. H. Gröschel *et al.*, *Nat. Commun.* **3**, 710 (2012).
13. W. Zhang *et al.*, *Science* **334**, 340–343 (2011).
14. R. Erhardt *et al.*, *Macromolecules* **34**, 1069–1075 (2001).
15. P. A. Rupar, L. Chabanne, M. A. Winnik, I. Manners, *Science* **337**, 559–562 (2012).
16. T. Muraoka, K. Kinbara, T. Aida, *Nature* **440**, 512–515 (2006).
17. E. W. Abel, N. J. Long, K. G. Orrell, A. G. Osborne, V. Šik, *J. Organomet. Chem.* **403**, 195–208 (1991).
18. A. N. Khlobystov *et al.*, *Coord. Chem. Rev.* **222**, 155–192 (2001).
19. D. Braga *et al.*, *Chem. Commun. (Camb.)* **10**, 1080–1081 (2002).
20. C. Y. Chen, J. Y. Zeng, H. M. Lee, *Inorg. Chim. Acta* **360**, 21–30 (2007).
21. S. Shin *et al.*, *J. Am. Chem. Soc.* **135**, 2156–2159 (2013).
22. C. Tarabout *et al.*, *Proc. Natl. Acad. Sci. U.S.A.* **108**, 7679–7684 (2011).
23. G. Oster, D. P. Riley, *Acta Crystallogr.* **5**, 272–276 (1952).
24. Materials and methods are available as supplementary materials on *Science* Online.
25. I. O. Shklyarevskiy *et al.*, *Langmuir* **21**, 2108–2112 (2005).
26. W. H. de Jeu, in *Physical Properties of Liquid Crystalline Materials* (Gordon and Breach, New York, 1980), pp. 24–33.
27. W. Jin *et al.*, *Proc. Natl. Acad. Sci. U.S.A.* **102**, 10801–10806 (2005).
28. D. M. Eisele *et al.*, *Nat. Chem.* **4**, 655–662 (2012).
29. H. Schumann, A. Lentz, R. Weimann, *J. Organomet. Chem.* **487**, 245–252 (1995).
30. T. Muraoka, K. Kinbara, Y. Kobayashi, T. Aida, *J. Am. Chem. Soc.* **125**, 5612–5613 (2003).

Acknowledgments: T.F. thanks the Japan Society for the Promotion of Science Young Scientist Fellowship (23•9024). We acknowledge Grant-in-Aid for Specially Promoted Research on "Physically Perturbed Assembly for Tailoring High-Performance Soft Materials with Controlled Macroscopic Structural Anisotropy" (25000005) and for Scientific Research on Innovative Areas "Coordination Programming" (21108012). The synchrotron x-ray diffraction experiments were performed at the BL45XU in the SPring-8 with the approval of the RIKEN SPring-8 Center (proposal 20130079).

Supplementary Materials

www.sciencemag.org/content/344/6183/499/suppl/DC1
Materials and Methods
Figs. S1 to S26
Tables S1 to S3
References (*31*–*41*)

11 February 2014; accepted 26 March 2014
Published online 10 April 2014;
10.1126/science.1252120

Vibrationally Promoted Dissociation of Water on Ni(111)

P. Morten Hundt,[1]† Bin Jiang,[2]† Maarten E. van Reijzen,[1] Hua Guo,[2]* Rainer D. Beck[1]*

Water dissociation on transition-metal catalysts is an important step in steam reforming and the water-gas shift reaction. To probe the effect of translational and vibrational activation on this important heterogeneous reaction, we performed state-resolved gas/surface reactivity measurements for the dissociative chemisorption of D_2O on Ni(111), using molecular beam techniques. The reaction occurs via a direct pathway, because both the translational and vibrational energies promote the dissociation. The experimentally measured initial sticking probabilities were used to calibrate a first-principles potential energy surface based on density functional theory. Quantum dynamical calculations on the scaled potential energy surface reproduced the experimental results semiquantitatively. The larger increase of the dissociation probability by vibrational excitation than by translation per unit of energy is consistent with a late barrier along the O-D stretch reaction coordinate.

Water dissociation on transition-metal surfaces (*1*, *2*) is an essential part in the steam reforming process used on a large scale by the chemical industry to convert natural gas [methane (CH_4)] to H. In the first step, CH_4 and water vapor (steam) react on a Ni catalyst to produce a mixture of CO and H_2 (syngas). The CO is reacted again with water, and this water-gas shift reaction produces additional H_2 and CO_2. The H_2 is used as a clean fuel and for the industrial production of important chemicals such as ammonia and methanol. In both reactions, the dissociative chemisorption of H_2O on the catalyst surface to form chemisorbed OH(ads) and H(ads) is an essential fundamental step, so an in-depth understanding of the adsorption and dissociation of water on a transition-metal catalyst surface is highly desirable. Although the dissociative chemisorption of CH_4 has been extensively studied by quantum-state–resolved experiments (*3*–*9*), until now, few experimental studies of water dissociation on transition metals have been available (*2*). We report a quantum-state–resolved study for D_2O dissociative chemisorption on Ni(111), jointly with a quantum-dynamical

[1]Laboratoire de Chimie Physique Moléculaire, Ecole Polytechnique Fédérale de Lausanne, 1015 Lausanne, Switzerland. [2]Department of Chemistry and Chemical Biology, University of New Mexico, Albuquerque, NM 87131, USA.

*Corresponding author. E-mail: hguo@unm.edu (H.G.); rainer.beck@epfl.ch (R.D.B.)
†These authors contributed equally to this work.

investigation on a density functional theory (DFT)–based global potential energy surface (PES), with the aim of progressing toward a predictive understanding of this important reaction.

Dissociative chemisorption of both water and CH_4 on Ni surfaces occurs via a direct mechanism in which the incident molecules either dissociate on the surface on initial impact or are scattered back to the gas phase intact. For CH_4, earlier experiments have shown that the dissociative chemisorption is activated by both the translational and vibrational energy of the incident molecule [(*3*) and references therein]. Quantum-state–resolved experiments for CH_4 have later revealed several signatures of nonstatistical reaction dynamics. The dissociation reaction of several isotopologues of CH_4 on Ni and Pt surfaces was observed to be both mode-specific (*4*–*6*) and bond-selective (*7*, *8*). Furthermore, the vibrational efficacy $\eta(v_i)$, which compares reactivity enhancement for vibrational excitation of a specific quantum state v_i with the effect of increasing the incident translational energy by an equivalent amount, took values both above and below unity, depending on the vibrational state of CH_4 and the type of metal surface. Finally, experiments with laser-aligned incident CH_4 molecules uncovered a hitherto unexplained steric effect in the CH_4 reactivity on several different Ni surfaces (*9*, *10*). All these observations show the inadequacy of statistical models (*11*, *12*) for a realistic microscopic description of CH_4 chemisorption and provide stringent tests for classical and/or quantum-dynamics calculations on multidimensional PESs (*13*–*16*).

Recently, theoretical studies of water dissociative chemisorption have predicted strong mode specificity (*17*), bond selectivity (*18*), and steric effects (*19*, *20*) for water on Cu(111) and Ni(111) (*21*). In addition, experiments have demonstrated mode specificity and bond selectivity in bimolecular reactions of water with H (*22*–*24*) and Cl atoms (*25*) in the gas phase. The strong vibrational enhancement in these gas-phase processes has been attributed, according to Polanyi's rules (*26*), to the "late" barrier along the reaction path, a characteristic that is shared by the dissociative chemisorption of both CH_4 and water. Challenged by the theoretical predictions, we investigated the effects of translational and vibrational excitation on the dissociation probability of water on the Ni(111) surface. We used single- and double-resonance excitation by infrared (IR) laser pumping in a molecular beam (*27*) to prepare surface-incident D_2O selectively either with one or two vibrational quanta of antisymmetric O-D stretch excitation (ν_3 or $2\nu_3$) in order to measure its state-resolved dissociation probability on a Ni(111) single-crystal surface. Such a selective quantum-state preparation by population inversion only became feasible recently for D_2O because of the availability of tunable high-power IR laser sources that emit light in the O-D stretching region. To better understand the experimental results, a six-dimensional (6D) PES was developed based on a large number of DFT points on Ni(111), and the dissociative chemisorption dynamics of D_2O were investigated with a 6D quantum wave-packet method. As demonstrated below, the synergistic interplay between state-resolved experiment and high-level quantum theory leads to a much deeper understanding of this prototypical surface reaction.

Details of the experimental setup have been described in previous publications (*28*, *29*). Briefly, a continuous molecular beam of D_2O was generated by skimming a supersonic expansion of a gas mixture of 3% D_2O in He obtained by bubbling He gas through a reservoir containing liquid D_2O. D_2O was chosen over H_2O because our available IR sources only allowed the preparation of O-D stretching states. The molecular beam speed was controlled by variation of the nozzle temperature and was measured using a fast chopper wheel together with a quadrupole mass spectrometer located in the molecular beam path. The surface-incident D_2O molecules were prepared with either one or two quanta of antisymmetric O-D stretch vibration (ν_3) by rapid adiabatic passage (*27*) with IR radiation from two optical parametric oscillators for either single- or double-resonance excitation. We measured state-resolved reaction probabilities on a clean Ni(111) surface [surface temperature ($T_{surface}$) = 300 K] for the dissociative chemisorption of D_2O according to $D_2O(v,J,E_t) \rightarrow OD(ads) + D(ads)$ (v and J designate the vibrational and rotational quantum states of the D_2O reactant) as a function of incident translational energy (E_t) for the ν_3 and $2\nu_3$ states, as well as without laser excitation by quantifying the coverage of the surface-bound OD(ads) product with Auger electron spectroscopy (AES) resulting from a known dose of incident D_2O [additional experimental details can be found in the supplementary materials (SM) (*30*)].

For a theoretical description of water dissociation on Ni(111), we developed a 6D flat rigid surface model (Fig. 1), following our earlier work on Cu(111) (*17*). The 6D global PES was constructed from ~22,000 spin-polarized DFT points on a three-layer slab with a 2 × 2 unit cell, using the PW91 functional (*31*) implemented in VASP (the Vienna Ab-initio Simulation Package) (*32*, *33*). These points were fit using the permutation-invariant polynomial approach (*34*), with a root mean square deviation of 2.0 kJ/mol for the dynamically relevant region (points below 145 kJ/mol). The resulting PES reproduces the geometries, energies, and frequencies for stationary points obtained in the DFT calculations quite well and are also consistent with earlier electronic structure calculations (*30*). The quantum dynamics were represented in Jacobi coordinates (shown in Fig. 1) by a 6D Chebyshev real wave-packet method (*20*, *35*). Specifically, an initial wave packet was launched for a rovibrational state of reactant (D_2O) above the surface and propagated on the PES using the Chebyshev three-term recursion formula. The total reaction probability was computed with a flux method on a dividing surface placed beyond the saddle point. The effects of surface corrugation, impact site, and lattice motion are approximately treated based on the approaches of Jackson and co-workers (*14*, *36*, *37*). A more detailed description of the theoretical calculations is given in the SM (*30*).

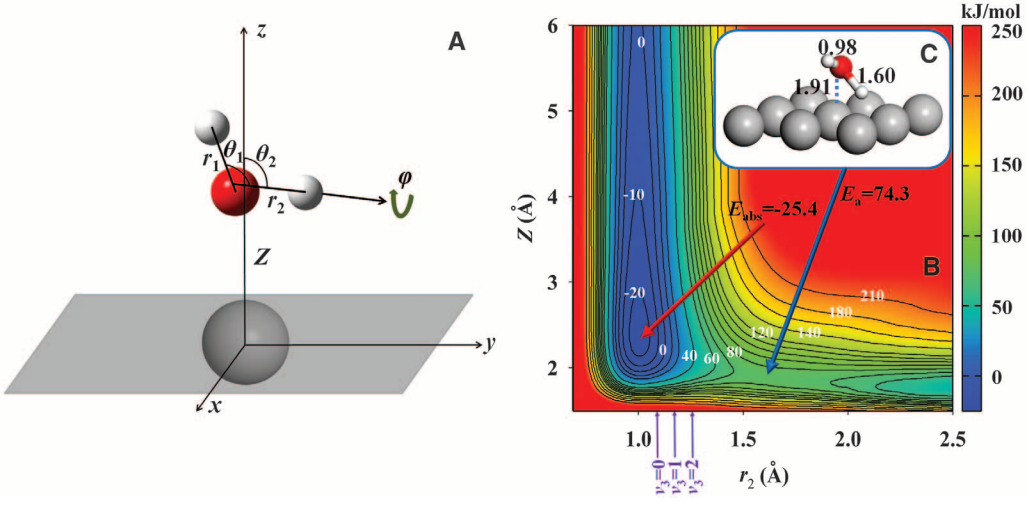

Fig. 1. Potential energy surface. (**A**) Definition of the six Jacobi coordinates used in the theoretical model, (**B**) Contour plot of the 6D scaled PES as a function of Z and r_2, with all other coordinates optimized. The adsorption well and transition state are indicated in red and blue arrows with the corresponding energies. (**C**) The geometry of the transition state in the Jacobi coordinates r_1 = 0.98 Å, r_2 = 1.60 Å, Z = 1.91 Å (where r_1 is the bond length of the nondissociative OD bond, r_2 is the distance between the centers of mass of OD and D, and Z is the distance between the D_2O center of mass and the surface). The contours are in kilojoules per mole relative to the D_2O in the gas phase, and the outer turning points of the O-D bond for ν_3 = 0, 1, and 2 are indicated by purple arrows.

Figure 2 shows a comparison of the AES-detected OD coverage on the Ni(111) surface resulting from two D_2O depositions at E_t = 36.5 kJ/mol with and without laser excitation of the incident molecular beam. For the laser-off deposition, the absence of substantial OD coverage in the region where the molecular beam struck the Ni(111) surface (Fig. 2, right, labeled laser-off) shows that 36.5 kJ/mol of translational energy normal to the surface was insufficient for the incident D_2O to overcome the reaction barrier and to dissociate to produce OD(ads). For the laser-on deposition (Fig. 2, left, labeled laser-on), rovibrational excitation of 30% of the incident D_2O in the molecular beam with two quanta of the antisymmetric O-D stretch normal mode ($2\nu_3$) added 66.8 kJ/mol of vibrational energy to the reactant molecules and led to dissociation of 0.05% of the incident vibrationally excited D_2O ($2\nu_3$) as detected by the AES signal. The data presented in Fig. 2 show that water dissociation on Ni(111) is strongly activated by vibrational energy, which is consistent with the results of earlier simulations for the H_2O/Cu(111) system (*17*).

In order to probe for translational activation and to compare the effect of translational and vibrational energy, we performed reactivity measurements at several incident energies E_t in the range of 36.5 to 75 kJ/mol for ν_3 and $2\nu_3$ excitation of the incident D_2O and in the range of 55 to 75 kJ/mol without laser excitation. The average E_t of the molecular beam was controlled by changing the temperature of the expansion nozzle T_n in steps of 100 K from 373 to 773 K. Figure 3 shows a summary of our state-resolved D_2O reactivity measurements on a Ni(111) surface at a surface temperature of 300 K. Because we varied E_t by increasing T_n, and vibrational relaxation in a supersonic expansion is inefficient, the measured laser-off D_2O reactivity contained an unknown contribution from the dissociation of vibrationally excited D_2O from the hot nozzle. Thus, the measured laser-off reactivity can only be taken as an upper limit to the $v = 0$ reactivity, which, depending on the fraction of vibrationally excited D_2O and the vibrational efficacies, may be substantially lower. The experimental state-resolved ν_3 and $2\nu_3$ reactivities were not affected by the effect of heating the expansion nozzle, because they were obtained from the difference between laser-on and laser-off measurements, where the contributions of thermally excited vibrations cancel.

For comparison of the effect of translational and vibrational excitation, we parameterized the state-resolved data by fitting S-shaped reactivity curves, initially suggested by Luntz (*38*), to each of the ν_3 and $2\nu_3$ data sets. For the laser-off data, which represent an average of different vibrational states populated at a given T_n, the same analysis is not suitable. These S-shaped curves are based on the assumption of a Gaussian distribution of reaction barrier heights of width W about an average barrier E_0. The width of the barrier reflects the combined effect of different initial orientations of the incident D_2O, the distribution of impact sites of D_2O within the unit cell of the Ni(111) surface lattice, and the distribution of thermal surface atom displacement along the surface normal. The fitted curves are represented by the dotted lines in Fig. 3. The horizontal shift of 37 kJ/mol between the state-resolved S-shaped reactivity curves for ν_3 and $2\nu_3$ excitation along the E_t axis can be used to compare the effects of translational and vibrational energy on the reaction probability. The ratio of the translational energy shift to the vibrational energy of 33.2 kJ/mol gives the vibrational efficacy $\eta(2\nu_3\text{-}\nu_3)$. For the second quantum of ν_3 excitation, the efficacy is 1.1 ± 0.05, indicating that vibrational excitation from ν_3 to $2\nu_3$ is more efficient in promoting reactivity than is adding an equal amount of translational energy to the incident molecule. Because the efficacy for the second quantum of ν_3 excitation is expected to be lower than that of the first (*3*), we would expect $\eta(\nu_3)$ to be larger than 1.1, although we cannot determine it directly from the laser-off data for the reasons stated above. Given such a large effect of vibrational energy on the reactivity, we can conclude that the laser-off reactivity is dominated by thermal vibrationally excited molecules, which is consistent with the theoretical results presented below.

The state-resolved reactivity data for ν_3 and $2\nu_3$ excitation reported here provide stringent tests for theoretical models. The 6D model used here contains all important degrees of freedom for water dissociative chemisorption, including all three vibrational modes of D_2O. Although the theoretical sticking probabilities calculated on the PW91 PES display appreciable mode specificity, they were systematically larger than the experimental results. The discrepancy was attributed to the underestimation of the barrier height (64.6 kJ/mol relative to free H_2O) by the PW91 functional. Indeed, a higher (99.1 kJ/mol) barrier was found with

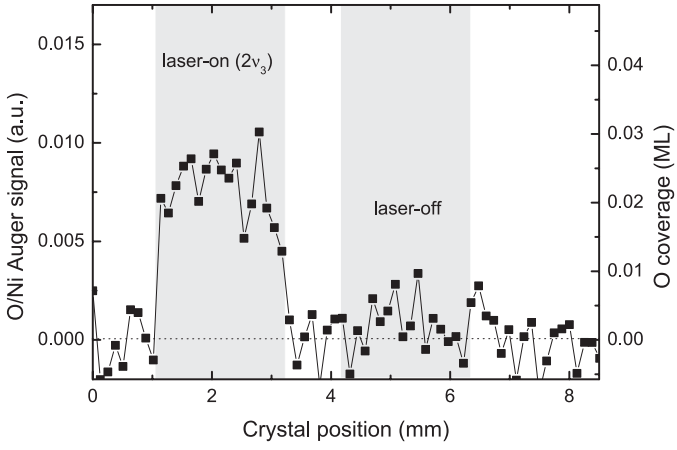

Fig. 2. Product detection. Auger-detected surface-bound OD after depositions of a molecular beam of D_2O (36.5 kJ/mol) with and without selective rovibrational excitation. $2\nu_3$ excitation is achieved by a sequential double-resonance pumping of a ν_3-$R_{11}(1)$ transition, followed by an $R_{12}(2)$ transition from ν_3 to $2\nu_3$. The surface temperature was 300 K. a.u., arbitrary units; ML, monolayer units.

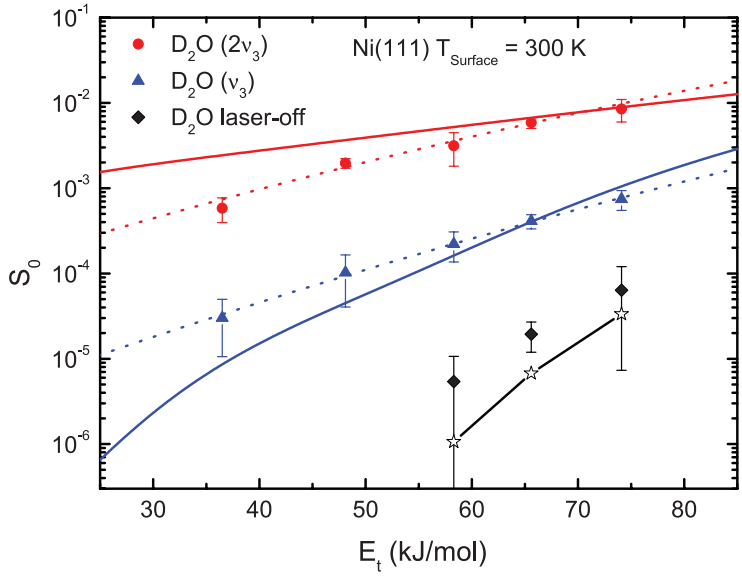

Fig. 3. State-resolved initial dissociation probabilities of D_2O on a Ni(111) surface. The solid points represent the experimental data, and the dotted lines are fitted S-shaped reactivity curves [see text and SM (*30*)]. Solid lines are the results of quantum dynamics calculations on the 6D scaled PES, and the open stars are calculated laser-off reactivities, including the thermal vibrational excitation for the nozzle temperature used in each experiment.

the revised Perdew-Burke-Ernzerhof (RPBE) functional (*39*). Similar observations have been reported by Kroes and co-workers on H_2 dissociative chemisorption, and these authors have corrected the PES using a combination of PW91 and RPBE functionals (*40*, *41*). We elected to scale the PW91 PES with a simple function of the distance (Z) between D_2O and the surface $\{V_{scaled} = V \times [1 + \exp(-\lambda Z)]$, with scaling parameter $\lambda = 1$ Å$^{-1}\}$, which resulted in a barrier of 74.3 kJ/mol, between the values predicted by the PW91 and RPBE functionals. The resulting PES shown in Fig. 1 features a saddle point with an elongated O-D bond (1.54 Å versus 0.97 Å for the equilibrium in D_2O), similar to that for H_2O on Cu(111) (*17*).

The simulations of the laser-off data were done with nozzle temperatures of 573, 673, and 773 K, at which several vibrational states of D_2O are significantly populated. The calculated sticking probabilities are thus a Boltzmann average of the contributions from these states. This approach has been used previously by Kroes and co-workers in their studies for H_2 dissociative chemisorption processes (*42*). For the simulation of state-resolved experiments, only the specific vibrational state (ν_3 or $2\nu_3$) prepared by the IR laser is considered. The calculated sticking probabilities obtained on the scaled PES are compared with the experimental results in Fig. 3, reproducing both the promotional effects for the translational and vibrational modes. Quantitatively, the calculated sticking probabilities for the ν_3 and $2\nu_3$ excited D_2O are in good agreement with the experimental counterparts between 55 and 75 kJ/mol, but theory overestimates and underestimates the vibrational enhancement in the low- and high-energy wings, respectively. The discrepancies can probably be attributed to the approximately treated degrees of freedom and uncertainties in the DFT functionals. We emphasize that the experiment-theory agreement underscores the importance of experimental calibration of the theoretical model.

As discussed above, the experimental data alone are insufficient to provide a reliable ν_3 efficacy $\eta(\nu_3)$. Fortunately, theory complements experiment by providing estimates of the vibrational efficacies for all vibrational states. As shown in the SM (*30*), all three vibrational modes of D_2O promote the reaction more effectively than translation. As a result, even when the thermal populations of the excited vibrational states of D_2O are relatively small, the laser-off reactivity is dominated by these highly reactive states. Similar vibrational efficacies have also been found for the gas-phase reaction between H and stretch-excited H_2O, and the rate constants were likewise dominated by excited vibrational states (*43*).

The theoretical estimate of the vibrational efficacy $\eta(\nu_3)$ for the antisymmetric stretch is about 1.65 to 1.78, substantially larger than vibrational efficacies observed in CH_4 dissociative chemisorption on Ni surfaces, which fall in the range of 0.5 to 1.4 (*3*–*6*). The vibrational enhancement of the reactivity can be understood by the recently proposed sudden vector projection (SVP) model, which assumes that the reaction occurs in the sudden limit, and the enhancement of reactivity by a reactant mode reflects its coupling with the reaction coordinate at the transition state (*35*, *44*). Such coupling can be estimated by the projection of the reactant mode vector onto the reaction coordinate vector at the transition state. The high vibrational efficacy for D_2O dissociative chemisorption can be rationalized by the fact that the SVP projection for the antisymmetric stretching mode (0.65) is substantially larger than that for the translation (0.34). As discussed elsewhere (*44*), the stronger coupling between the reactant vibration and the reaction coordinate is related to the late barrier and thus is consistent with Polanyi's rules (*26*). Indeed, it is shown in Fig. 1 that the classical outer turning point of the $\nu_3 = 0$, 1, or 2 state progressively approaches the saddle point, allowing better access of the transition state.

There has been substantial progress in understanding dissociative chemisorption of diatomic molecules on metal surfaces in recent years (*45*). The theory-experiment agreement in these systems has reached an unprecedented level, thanks to the chemical accuracy (<1 kcal/mol) of the PESs (*41*). However, it is still extremely challenging to repeat such success for heterogeneous reactions involving polyatomic molecules. The in-depth understanding of the reaction dynamics for water dissociation provided by the present synergistic experimental-theoretical work has important implications in advancing our understanding and control of prototypical polyatomic surface reactions beyond their well-understood diatomic counterparts. The mode specificity demonstrated in the dissociative chemisorption of water on Ni(111) suggests that such a phenomenon is not restricted to CH_4 and might be quite prevalent in many surface reactions. A key determinant of mode specificity and bond selectivity is the slow rate of surface-induced intramolecular vibrational energy redistribution of the reactant, which is related to its sparse density of states (*46*). Both CH_4 and H_2O, and many other molecules, obviously possess these properties. More interestingly, the results presented here suggest that water dissociation in high-temperature (700° to 1100°C) steam reforming is dominated by Boltzmann populated excited vibrational states, thanks to their high vibrational efficacies. Further experimental and theoretical work will be needed to investigate mode specificity, bond selectivity, and steric effects in water chemisorption, with the goal of developing a predictive understanding of this important gas/surface reaction.

References and Notes

1. P. A. Thiel, T. E. Madey, *Surf. Sci. Rep.* **7**, 211–385 (1987).
2. M. A. Henderson, *Surf. Sci. Rep.* **46**, 1 (2002).
3. L. B. F. Juurlink, D. R. Killelea, A. L. Utz, *Prog. Surf. Sci.* **84**, 69–134 (2009).
4. R. D. Beck *et al.*, *Science* **302**, 98–100 (2003).
5. P. Maroni *et al.*, *Phys. Rev. Lett.* **94**, 246104 (2005).
6. L. B. F. Juurlink, R. R. Smith, D. R. Killelea, A. L. Utz, *Phys. Rev. Lett.* **94**, 208303 (2005).
7. D. R. Killelea, V. L. Campbell, N. S. Shuman, A. L. Utz, *Science* **319**, 790–793 (2008).
8. L. Chen, H. Ueta, R. Bisson, R. D. Beck, *Faraday Discuss.* **157**, 285–295, discussion 375–398 (2012).
9. B. L. Yoder, R. Bisson, R. D. Beck, *Science* **329**, 553–556 (2010).
10. B. L. Yoder, R. Bisson, P. Morten Hundt, R. D. Beck, *J. Chem. Phys.* **135**, 224703 (2011).
11. V. A. Ukraintsev, I. Harrison, *J. Chem. Phys.* **101**, 1564 (1994).
12. A. Bukoski, D. Blumling, I. Harrison, *J. Chem. Phys.* **118**, 843 (2003).
13. S. Nave, B. Jackson, *Phys. Rev. B* **81**, 233408 (2010).
14. B. Jackson, S. Nave, *J. Chem. Phys.* **135**, 114701 (2011).
15. B. Jiang *et al.*, *Chem. Sci.* **4**, 3249 (2013).
16. F. Nattino *et al.*, *J. Phys. Chem. Lett.* **5**, 1294–1299 (2014).
17. B. Jiang, X. Ren, D. Xie, H. Guo, *Proc. Natl. Acad. Sci. U.S.A.* **109**, 10224–10227 (2012).
18. B. Jiang, D. Xie, H. Guo, *Chem. Sci.* **4**, 503 (2013).
19. A. Mondal, H. Seenivasan, A. K. Tiwari, *J. Chem. Phys.* **137**, 094708 (2012).
20. B. Jiang, J. Li, D. Xie, H. Guo, *J. Chem. Phys.* **138**, 044704 (2013).
21. H. Seenivasan, A. K. Tiwari, *J. Chem. Phys.* **139**, 174707 (2013).
22. A. Sinha, M. C. Hsiao, F. F. Crim, *J. Chem. Phys.* **92**, 6333 (1990).
23. M. C. Hsiao, A. Sinha, F. F. Crim, *J. Phys. Chem.* **95**, 8263–8267 (1991).
24. M. J. Bronikowski, W. R. Simpson, R. N. Zare, *J. Phys. Chem.* **97**, 2194–2203 (1993).
25. A. Sinha, J. D. Thoemke, F. F. Crim, *J. Chem. Phys.* **96**, 372 (1992).
26. J. C. Polanyi, *Science* **236**, 680–690 (1987).
27. H. Chadwick, P. M. Hundt, M. E. van Reijzen, B. L. Yoder, R. D. Beck, *J. Chem. Phys.* **140**, 034321 (2014).
28. M. P. Schmid, P. Maroni, R. D. Beck, T. R. Rizzo, *Rev. Sci. Instrum.* **74**, 4110 (2003).
29. P. M. Hundt, R. Bisson, R. D. Beck, *J. Chem. Phys.* **137**, 074701 (2012).
30. Materials and methods are available as supplementary materials on *Science* Online.
31. J. P. Perdew, K. A. Jackson, M. R. Pederson, D. J. Singh, C. Fiolhais, *Phys. Rev. B* **46**, 6671–6687 (1992).
32. G. Kresse, J. Furthmuller, *Phys. Rev. B* **54**, 11169–11186 (1996).
33. G. Kresse, J. Furthmuller, *Comput. Mater. Sci.* **6**, 15–50 (1996).
34. J. M. Bowman, G. Czakó, B. Fu, *Phys. Chem. Chem. Phys.* **13**, 8094–8111 (2011).
35. B. Jiang, H. Guo, *J. Am. Chem. Soc.* **135**, 15251–15256 (2013).
36. D. Han, S. Nave, B. Jackson, *J. Phys. Chem. A* **117**, 8651–8659 (2013).
37. A. K. Tiwari, S. Nave, B. Jackson, *J. Chem. Phys.* **132**, 134702 (2010).
38. A. C. Luntz, *J. Chem. Phys.* **113**, 6901 (2000).
39. B. Hammer, L. B. Hansen, J. K. Nørskov, *Phys. Rev. B* **59**, 7413–7421 (1999).
40. G.-J. Kroes, *Phys. Chem. Chem. Phys.* **14**, 14966–14981 (2012).
41. C. Díaz *et al.*, *Science* **326**, 832–834 (2009).
42. L. Sementa *et al.*, *J. Chem. Phys.* **138**, 044708 (2013).
43. D. H. Zhang, M. A. Collins, S.-Y. Lee, *Science* **290**, 961–963 (2000).
44. B. Jiang, H. Guo, *J. Chem. Phys.* **138**, 234104 (2013).
45. G.-J. Kroes, *Science* **321**, 794–797 (2008).
46. D. R. Killelea, A. L. Utz, *Phys. Chem. Chem. Phys.* **15**, 20545–20554 (2013).

Acknowledgments: P.M.H., M.v.R., and R.D.B. gratefully acknowledge financial support from the Swiss National Science Foundation (grant no. 146487/1) and the Ecole Polytechnique Fédérale de Lausanne. B.J. and H.G. thank the U.S. NSF (grant no. CHE-0910828) for support. The experiments were done by the Lausanne group, and the theory was developed by the Albuquerque group.

Supplementary Materials

www.sciencemag.org/content/344/6183/504/suppl/DC1
Materials and Methods
Figs. S1 to S8
Tables S1 to S6
References (*47*–*83*)

24 January 2014; accepted 3 April 2014
10.1126/science.1251277